ACERP: Vol. 2, No. 4, (Fall 2016) 25-31

Advanced Ceramics Progress

Research Article

Journal Homepage: www.acerp.ir

Investigation of HF/H_2O_2 Concentration Effect on Structural and Antireflection Properties of Porous Silicon Prepared by Metal-Assisted Chemical Etching Process for Photovoltaic Applications

Sh. Mahmoudi[a], M.J. Eshraghi*[a], B. Yarmand[b], N. Naderi[a]

[a]*Department of Semiconductor, Materials and Energy Research Center, Karaj, Iran*
[b]*Department of Nanotechnology and Advanced Materials, Materials and Energy Research Center, Karaj, Iran*

PAPER INFO

Paper history:
Received 21 November 2016
Accepted in revised form 01 May 2017

Keywords:
Porous Silicon
HF/H_2O_2 Ratio
Metal-Assisted Chemical Etching
Anti-Reflection Properties

ABSTRACT

Porous silicon was successfully prepared using metal-assisted chemical etching method. The Effect of HF/H_2O_2 concentrations on the porosity type and size was investigated as an effective parameter in etching solution. Various structures can be synthesized by implementing different regimes of ρ which is the function of molar ratio of HF/H_2O_2. It is found that the best achieved etching rate is equal to 85%. Field Emission Electron Microscopy (FE-SEM) confirmed that all etched samples have porous structure and the sample which was immersed into HF/H_2O_2 with molar ratio of 7/3.53 has the smallest porosities. The average roughness of 288 nm and reflectivity as low as 7% could be achieved using this molar ratio. The Raman peak appeared at 520.09 cm^{-1} confirmed that there weren't any defect and stress in the porous structure. Current density-Voltage characterization was done for investigation important parameters of the prepared solar cells which had different structures. So it was shown that the porous sample immersed into HF/H_2O_2 with molar ratio of 7/3.53 had J_{sc} and V_{oc} equal to 0.118Acm^{-2} and 0.56V, respectively. The prepared porous silicon is a potential candidate for replacing antireflective layers in photovoltaic devices because of its low production cost, high antireflective property, and possibility of integration process relative to other antireflection layers.

1. INTRODUCTION

Silicon nanostructures (SNs) are important materials which form the basis of many systems such as nano-electronics, optoelectronics, energy conversion, solar cells, chemical and biosensors [1-7]. SNs due to their special features are more interesting than bulk silicon. Orientation of nanostructures, their quality, strain, and crystallite size are important parameters which play important role in determining the properties and applications of SNs for making various devices [5, 8-11]. Porous silicon (PS) has been considered as a potential structure for enhancing the light-trapping sufficiency in visible spectra which is practical for applications such as antireflection coating, high performance solar cells, and other optical devices [12] . For a long time, silicon has been propounded as an inappropriate material for optoelectronic applications because bulk silicon emits almost every beneficial light due to its indirect band gap nature [13]. This opinion was changed after discovery of bright emission from PS and nanocrystals [14]. In 1990s, PS layer attracted comprehensive researchers attention after discovery of light emitting properties of nano PS in visible region by L. Canham, who showed room temperature photoluminescence of an anodized p-type silicon wafer [15, 16] . PS has superior scientific and technological portions because of its abundant applications. They are being used in solar cells, due to its combination of light trapping, antireflection properties and light conversion ability [17]. PS due to its broad band gap, wide absorption spectrum, wide optical transmission range (700–1000 nm), lower effective refractive index, and surface roughening has been appeared as an absorbing material in electronic and optoelectronic fields. The amount of light reflection from the surface is the principal hindrance for increasing the solar cell efficiency. The silicon refractive index is 3.48 which prevents electron-hole pair generation and results in reduced efficiency of photovoltaic devices. Antireflection coatings (ARC) are able to decrease surface reflection, enhance conversion efficiency, develop the life of devices and improve the electro physical and characteristics of photovoltaic devices. PSs

*Corresponding Author's Email: eshr56@gmail.com (M.J. Eshraghi)

due to their efficient ARC and other properties such as band gap broadening, wide absorption spectrum, and optical transmission range (700-1000nm) are useful in solar cell applications [18]. SNs are made by different approaches that can be divided into two general categories (bottom-up and top-down). The most prominent method in bottom-up approach is based on vapor-liquid-solid growth [19-24]. Top-down approach can be divided into wet and dry etching method. Etching process with inductively coupled plasma is the most common dry etching method; while electrochemical etching and metal-assisted chemical etching are subsets of wet etching. Inductively coupled plasma and vapor-liquid-solid procedures require complex equipment and machines. Moreover, in these procedures it is required to use high purity gases, vacuum systems, and high temperature (or magnetic coil with high power) which makes them inappropriate for industrial uses. Electrochemical etching method requires applying external potential in specially designed electrochemical cells using platinum electrodes which increases the cost and complexity of this approach [25, 26]. Metal-assisted chemical etching (MACE) have been widely investigated as an easy, cheap, and reliable method for fabricating porous silicon [27, 28]. This method can create uniform layers of porous silicon (PS) without applying bias voltage which would be free of any substantial limitations on the characteristics of the fabricated structures. Chiappini et al. reported the synthesis of biodegradable porous silicon barcode nanowires by metal-assisted electroless etching of single crystal silicon with resistivity being in range of 0.0008 to 10Ω.cm. They developed phase diagrams for different nanostructures as a function of metal catalyst, H_2O_2 concentration, ethanol concentration, and silicon resistivity [29]. Xing Zhong et al. presented a systematic study to elucidate the mechanism responsible for formation of porous silicon nanowires in two-step silver-assisted electroless chemical etching method. They investigated effects of multiple experimental parameters including resistivity of the starting silicon wafer, concentration of oxidant (H_2O_2) and amount of silver catalyst on porosity. Their study showed a consistent trend that the porosity was increased with increase in wafer conductivity (dopant concentration) and oxidant (H_2O_2) concentration. They further demonstrated that silver ions, formed by the oxidation of silver, could diffuse upwards and renucleate on sidewalls of the nanowires to initiate new etching pathways to produce a porous structure [30]. The MACE method is divided to two different steps. Firstly, noble metal nanoparticles such as Ag nanoparticles are deposited on Si surface by immersing it into HF aqueous solution. Relative metallization is based on the following reaction:

$$Ag^+ + e^- \rightarrow Ag \quad E_0 = +0.79V/NHE \qquad (1)$$

Finally, wafers are etched into aqueous solution containing HF and an oxidizing agent such as H_2O_2 (Eq. (2)).

$$Si + 4HF_2^- \rightarrow SiF_6^{2-} + 2HF + H_2 + 2e^- \qquad (2)$$

$$E_0 = -1.2\ V/NHE$$

In MACE method, pattern of etched silicon nanostructure can be controlled by various parameters such as the type and morphology of noble metal (catalyst), the chemical composition of etching solution, the silicon substrate doping type and density, and external field application. In this method, orientation of SNs (e.g. nanowires and porosities) relative to substrate could also be controlled by MACE method [28]. Specially, thickness of porous layers can be controlled from nanometer-scale up to micrometer-scale via MACE [31, 32]. Some details of the MACE process have been developed by Li and Bohn for the first time. They deposited thin layer of noble metals (e.g. Ag, Au, Cu,…) on Si substrate using sputtering method and immersed the loaded substrate into a solution containing ethanol, hydrogen peroxide (H_2O_2), and hydrofluoric acid (HF) for creating porosity which led to the creation of direct and columnar structures [33]. Essence of this work is engineering the porous silicon reflectance through porosity control by varying the etching rate which is a function of etchant solution constituents (HF/H_2O_2). The etchant solution constituent effect on the structure and morphology of porous layers have been investigated as one of the most effective parameters to achieve the lowest reflection from the surface [28]. Furthermore, we have fabricated different silicon solar cells with and without porous substrates for comparing their characteristics and structures.

2. EXPERIMENTAL

Single crystal silicon wafers with (100) orientation doped with boron (p-type) having resistance of about 1-3 Ω.cm (Bayern, Germany) were used. The wafers were cleaved into $1\times1cm^2$pieces. Substrates were immersed into a solution containing HNO_3 (65%, Merck)/HF (40%, Merck)/CH_3COOH (99%, Merck) with volume ratios of 75/10/25 for 15 min prior to use. For removing native oxides on substrates, samples were immersed into Ethanol (96%, Merck) and HF 5% for 10 min and 5 min, respectively. Chemical metallization of silver particles on surface of the samples was performed by immersing sample in a mixture of HF (0.14M) and $AgNO_3$ (5×10^{-4}M) for 3 min. Afterwards the samples were immersed into a solution containing H_2O_2 (35%, Merck)/HF (40%)/Deionized water (DIW) for penetration of silver particles and creation of primary passive porous layer. When the etching process was started, the beaker bubbles were formed on the sample surface. Then the samples were rinsed by DIW and

dried at 100 ℃ for 10 min. Potassium hydroxide (KOH) 1M solution was used for creating post-passive porous layer for 60s. After second washing process, the samples were dried at 100 ℃ for 10 min. Finally, silver particles were removed by immersion into HF/HNO_3 solution with equal ratio for 2 min. In order to fabricate solar cells, the aqueous solution of phosphoric acid (H_3PO_4) was sprayed on porous and nonporous substrates. After that, they were kept in furnace at 910°C in which the diffusion could be done. Then the substrates were immersed into aqueous solution of HF 5% for removing the phosphosilica glass on surfaces. Finally, the front and rear contacts were deposited on substrates by evaporation method. The uniformity of surface samples was characterized via optical microscopy (OM, Olympus BX61). The morphology of samples was imaged by field emission scanning electron microscopy (FE-SEM, MIRA3 TESCAN). Energy dispersive X-ray spectroscopy (EDS) was utilized for semi-quantitative characterization of the elements existing on surface of the samples and estimating the size of metalized nanoparticles on surface. Digimizer image analysis software was used for accurate measurement of nano-sized silver particles. Average roughness and root mean square (RMS) surface slope were investigated using atomic force microscopy (AFM, Dualscope/Rasterscope C26, DME). Anti-reflective properties of the samples were analyzed with Spectrophotometer (Phystec co). Raman microscopy (SENTRA) was used for analyzing structure and the residual stresses in the structures. The J-V characteristics were determined by I-V tracer (Keytely).

3. RESULTS AND DISCUSSIONS

Fig. 1a shows the FE-SEM images of Si samples after metallization with silver particles. Silver nano spheres are stacked almost uniformly on the Si surface. The average size of silver nano spheres calculated using digimizer software was determined to be in the range of 20-150 nm. The average distance of nano spheres was estimated to be around 121 nm. The effective parameters in silver nano sphere deposition are temperature, metallization time, and salt-metal concentration. In Fig. 1b, EDS analysis results indicate that the gross combination was not formed on the substrate surface. Presence of small amounts of oxygen on the surface could be due to the partial oxidation of silver or Si substrate in the environment. The deposition causes performance of galvanic displacement: the silver ions are oxidizing agents for silicon substrates and are decreased while oxidizing silicon into SiO_2 [34].

Uniformity of sample surfaces which were immersed into etch solutions with different ratios of HF/H_2O_2 is characterized by optical microscopy (OM) at 700×700 μm^2 images in Fig. 2. Increasing the ratio of H_2O_2 to value of 3.53M resulted the most uniform surface for sample 3. According to pores measurements performed by digimizer software, the pore sizes are decreased by increasing ratio of H_2O_2 in etching solution (Table 1).

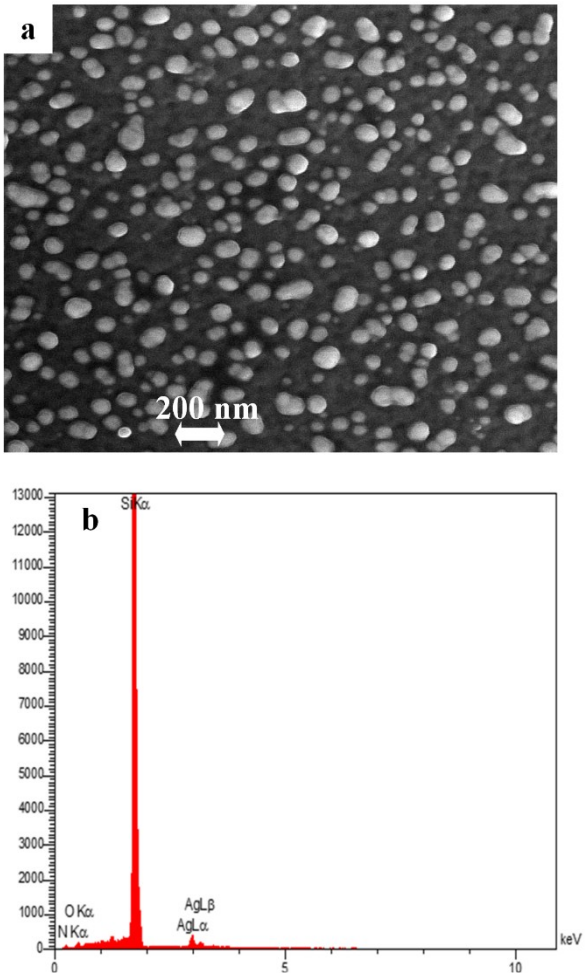

Figure 1. (a) FE-SEM image of silver nanoparticles coated on a silicon substrate, and (b) EDS analysis image of the sample surface

TABLE 1. Combination of etching solution and pore sizes of the silicon wafers

samples	Molar ratio of $HF:H_2O_2$ in etching solution	Average Pore size (nm)
sample1	7:2.32	352
sample 2	7:2.82	233
sample 3	7:3.53	177

Also, in [35], $[H_2O]$ was kept constant in $\rho=([HF])/([HF+H_2O_2])$. So we consider the ratio between the H_2O_2 and HF concentrations as a key parameter that etch rate is a function of molar ratio ρ. Since ρ is described in different regimes that effect pore

formations, we varied the amount of H_2O because it is not more important than ratio of H_2O_2 /HF.

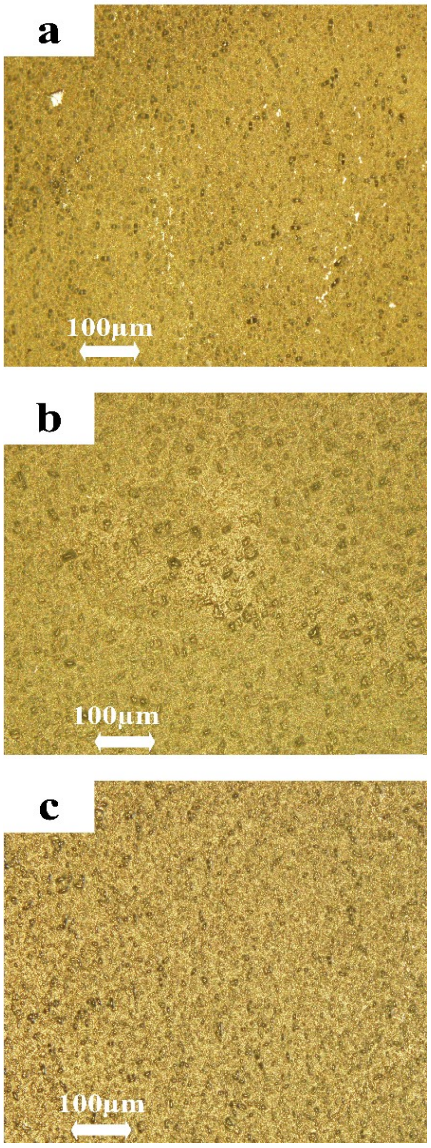

Figure 2. OM images of the etched surface of the samples in different concentrations of etching solutions; (a) sample 1, (b) sample 2, and (c) sample 3

TABLE 2. Specifications calculated from morphology of porous samples prepared at different concentrations of etching solution

Samples	Ratioof $HF:H_2O_2$in etching solution	Slope of root mean square profile (RMS)	Roughness ratio (nm)
Sample1	7:2.32	0.71	217
Sample2	7:2.82	0.68	268
Sample3	7:3.53	0.54	288

Fig. 5 shows the reflection spectra of visible beam with incidence and reflection angles being at 0°. This measurement is performed for the etched samples at different HF/H_2O_2 ratio with respect to the standard reflection sample.

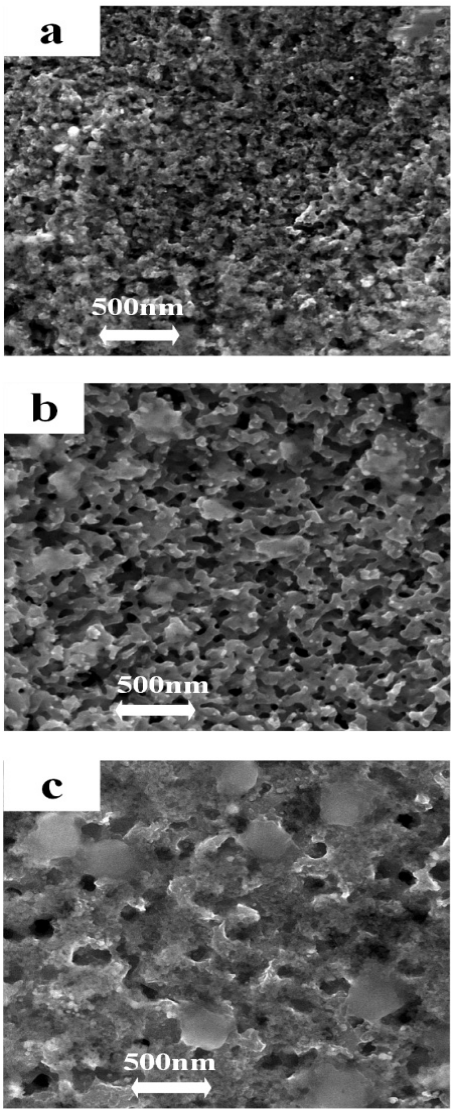

Figure 3. FE-SEM images showing the etched surface of the samples in different concentrations of etching solutions; (a) sample 1, (b) sample 2, and (c) sample 3

As can be seen the third sample has the effective reflectance around 7% which is the lowest reflection value among the prepared samples. According to the results reported in Table 1, this sample has the lowest average pore size so that trapping of sun light and surface reflection could approach the lowest level. According to Fig. 5, the first sample also shows the highest surface reflection which is related to largest pore sizes. Thus, the third sample with the lowest surface reflection is the best sample among the prepared samples which is able to provide the highest level of trapping.

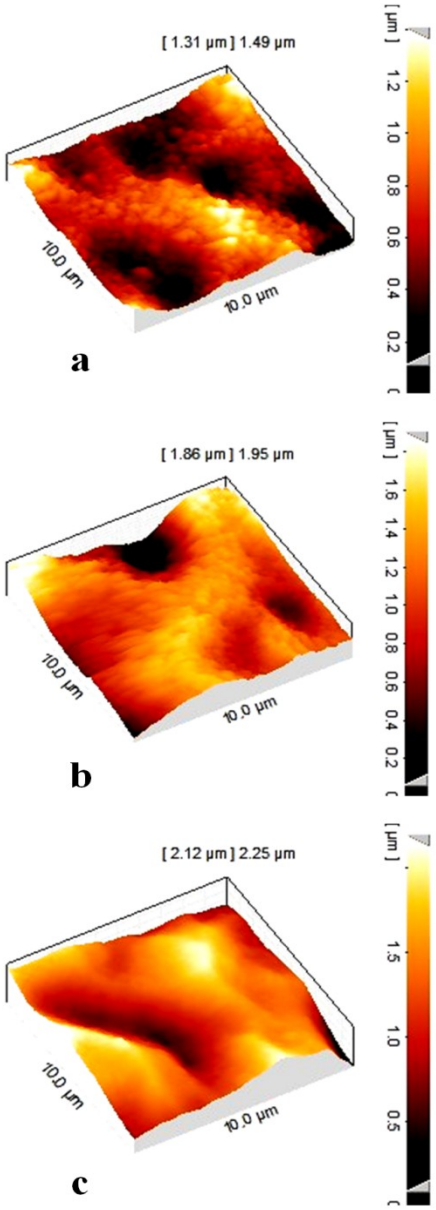

Figure 4. AFM images of porous silicon samples at different concentrations of etching solutions; (a) sample 1, (b) sample 2, and (c) sample 3

In Fig. 6a to 6d, Raman spectra of the as-casted single-crystal sample and the samples etched in three different concentrations are shown, respectively. It can be seen that full width half maximum (FWHM) of Raman peak is increased from 518.4 to 520.09 cm^{-1} by varying H_2O_2 concentration from 2.32 to 3.53M. Raman intensity for porous silicon is around 20% stronger than that of the single-crystalline silicon which is due to surface optimization or resonance effect [36, 37]. Raman spectra of the porous silicon layers can be analyzed by using phonon confinement model [38].

Disorder or finite size effects can result in relaxation of the momentum conservation, leading to a downshift and an asymmetric broadening of the first order Raman peak [39]. The wave number of first-order Raman band is 520.5cm^{-1} and its FWHM is 3cm^{-1} in absence of pressure and irregularities.

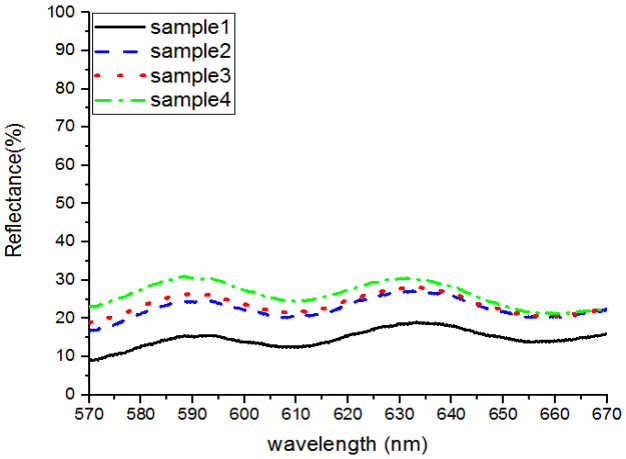

Figure 5. Optical reflection spectra of the silicon wafers etched in different concentrations of etching solutions relative to optical reflection spectra of the standard sample; (a) sample1, (b) sample2, and (c) sample3

It was found that when the third sample was immersed into the high concentration of etching solution of HF / H_2O_2, a peak at 520.09cm^{-1} was emerged. The results indicate the fact that the porous structure of this sample was created in silicon on a regular basis without any stress or disorder effects[36]. Among the these porous structures, the third one is the optimal structure and also has FWHM value equal to 9.6cm^{-1} which was the lowest among the prepared structures and also this sample possess the highest porosity value of 60%. However, for two other PSs, the Raman peak was shifted towards lower wavelengths and their FWHMs were larger.

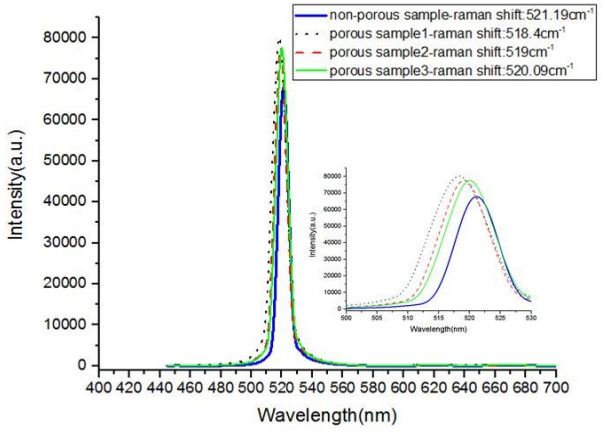

Figure 6. Raman spectra of PS samples in different concentrations of etching solutions (a) sample 1, (2) sample 2, (3) sample 3, and (4) non-porous sample

Current density-Voltage characteristics of the fabricated solar cells with and without porous structures are shown in Fig. 7. These curves show that the solar cell based on porous substrate has better J_{sc} and V_{oc} than non-porous silicon solar cell. The values of J_{sc} and V_{oc} of the prepared samples are reported in Table 3.

TABLE 3. J-V characterization of the porous and nonporous samples

Samples	Ratioof $HF:H_2O_2$in etching solution	Slope of root mean square profile (RMS)	Roughness ratio (nm)
Porous substrate	7/3.53	0.118	0.56
Non-porous substrate	-	0.05	0.55

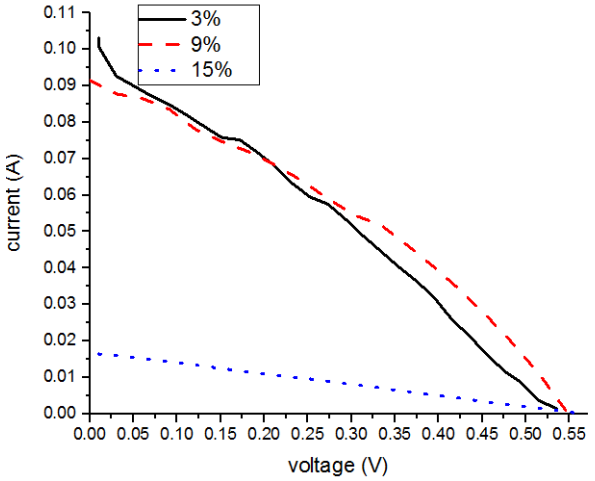

Figure 7. J-V cures of (solid line) porous substrate and (dash line) non porous substrate

4. CONCLUSION

Metal assisted-chemical etching method has been used for creating porous structures on Si wafers. The effect of variation of etching solution concentration on porosity and antireflection properties of porous silicon has been investigated. It is shown that by decreasing the HF/H_2O_2 ratio in etch solution from 3.53 to 2.32M, optical reflection varies from 7% to 25% at a wavelength of 600nm and the size of nanostructures varies from 177 to 352 nm. The lowest reflectance is related to the sample etched at HF/H_2O_2 concentration of 7/3.53 and is found to be 7% with respect to reflection standard at 600 nm. The average size of surface pores, the average roughness and RMS value for the sample with lowest reflectance were found to be 177nm, 288nm, and 0.54, respectively. The morphological studies show that all the fabricated porous silicon samples have great uniformity over the 700 µm× µm area.

For the sample with lowest reflectance the downshift and broadening of Raman peak toward the lowest energy indicates that the formed silicon layer is highly porous. Also this sample had a value FWHM of 9.6 cm^{-1} and relative to another structure has been had the lowest FWHM. In its Raman spectrum, the peak at 520.09 cm^{-1} was observed with its shape being nearly Lorentzian and it can be shown that this structure does not have any stress and defect. Since the light trapping is an essential problem in photovoltaic productions, optimized results have been applied in our research. Finally the solar cells fabricated with and without porous structures confirm all results about porous structures. The best porous substrate has great potential to offer the solar cell with best characteristics compared to nonporous substrate. The values of J_{sc} and V_{oc} are 0.118/0.05 Acm^{-2} and 0.56/0.55V for porous and nonporous substrates, respectively.

5. ACKNOWLEDGMENT

The authors thank material and energy research center supporting this research. Also, we thank Mr. Azizi for helping the fabrication of solar cells.

REFERENCES

1. Bastide, S., Quang, N.L., Monna, R., Celement, C.R., "Chemical etching of Si by Ag nanocatalysts in HF-H_2O_2: application to multicrystalline Si solar cell texturisation", ***Physica Status Solidi, (***2009), Vol. 26, No. 7, 1536-1540.
2. Chan, C.K., Peng, H., Liu, G., McIlwrath, K., Zhang, X.F., Huggins, R.A. and Cui, Y., "High-performance lithium battery anodes using silicon nanowires", ***Nature Nanotechnology,*** 2008. Vol. 3, No. 1, 31-35.
3. Goldberger, J., Hochbaum, A.I., Fan, R. and Yang, P., "Silicon vertically integrated nanowire field effect transistors", ***Nano Letters,*** Vol. 6, No. 5, (2006), 973-977.
4. Lipiński, M., Panek, P., Bastide, S. and Lévy-Clément , C., "Porous silicon antireflection coating by electrochemical and chemical etching for silicon solar cell manufacturing", ***Physica Status Solidi,*** Vol. 197, No. 2, (2003), 512-517.
5. Peng, K., Jie, J., Zhang, W. and Lee, S.T., "Silicon nanowires for rechargeable lithium-ion battery anodes", ***Applied Physics Letters,*** Vol. 93, No. 3 (2008), 033105.
6. Schmidt, V., Senz, S., Riel, H., Gösele, U., Riess, W. and Gösele , U., "Realization of a Silicon Nanowire Vertical Surround-Gate Field-Effect Transistor", ***Small,*** Vol. 2, No. 1, (2006), 85-88.
7. Tian, B., Zheng, X., Kempa, T.J., Fang, Y., Yu, N., Yu, G., Huang, J. and Lieber, C.M., "Coaxial silicon nanowires as solar cells and nanoelectronic power sources", ***Nature,*** Vol. 449, (2007), 885-889.
8. Buin, A.K., Verma, A., Svizhenko, A. and Anantram, M.P., "Significant enhancement of hole mobility in [110] silicon nanowires compared to electrons and bulk silicon", ***Nano Letters,*** Vol. 8, No. 2, (2008), 760-765.
9. Cloutier, S.G., Hsu, C.H., Kossyrev, P.A. and Xu, J., "Enhancement of Radiative Recombination in Silicon via Phonon Localization and Selection-Rule Breaking", ***Advanced Materials,*** Vol. 18, No. 7, (2006), 841-844.

10. Hong, K.-H., Kim, J., Lee, S.H. and Shin, J.K., "Strain-driven electronic band structure modulation of Si nanowires", ***Nano Letters,*** Vol. 8, No. 5, (2008), 1335-1340.
11. Lyons, D.M., Ryan, K.M., Morris, M.A. and Holmes, J.D., "Tailoring the optical properties of silicon nanowire arrays through strain", ***Nano Letters,*** Vol. 2, No. 8, (2002), 811-816.
12. Chen, C.-Y., Liu, R.-Y., Tseng, J.-C. and Hsu, P,-Y., "Uniform trench arrays with controllable tilted profiles using metal-assisted chemical etching", ***Applied Surface Science,*** Vol. 333, (2015), 152-156.
13. Hayashi, S. and Yamamoto, K., "Optical properties of Si-rich SiO 2 films in relation with embedded Si mesoscopic particles", ***Journal of Luminescence,*** Vol. 70, No. 1, (1996), 352-363.
14. Kim, B.-S., Kim, D.-I. and Lee, C.-W., "Photoluminescence from nano silicon materials prepared by photoelectrochemical methods", ***Journal of the Korean Physical Society,*** Vol. 38, No. 3, (2001), 245-250.
15. Delerue, C., Allan, G. and Lannoo, M., "Theoretical aspects of the luminescence of porous silicon", ***Physical Review B,*** Vol. 48, No. 15, (1993), 11024-11036.
16. Li, X., Coffer, J.L., Chen, Y., Pinizzotto, R.F., Newey, J. and Canham, L.T., "Transition metal complex-doped hydroxyapatite layers on porous silicon", ***Journal of the American Chemical Society,*** Vol. 120, No. 45, (1998), 11706-11709.
17. Chaoui, R., Mahmoudi, B., Ahmed, Y.S. and Mahmoudi, B., "Contribution of the photoluminescence effect of the stain etched porous silicon in improvement of screen printed silicon solar cell performance", ***Revue des Energies Renouvelables,*** Vol. 16, No. 2, (2013), 347-356.
18. Severiano, F., García, G., Castañeda, L.A., Gracia-Jiménez, J.M., Maldonado, A., Avendaño-Alejo, M., Coyopol, A. and Diaz, T., "Electroluminescent devices based on junctions of indium doped zinc oxide and porous silicon", ***Journal of Nanomaterials,*** Vol. 2014, (2014), 2-9.
19. Hofmann, S., Ducati, C., Neill, R.J., Piscanec, S. and Ferrari, A.C., "Gold catalyzed growth of silicon nanowires by plasma enhanced chemical vapor deposition", ***Journal of Applied Physics,*** Vol. 94, No. 9, (2003), 6005-6012.
20. Kwak, D., Cho, H. and Yang, W.-C., "Dimensional evolution of silicon nanowires synthesized by Au–Si island-catalyzed chemical vapor deposition", ***Physica E: Low-dimensional Systems and Nanostructures,*** Vol. 37, No. 1, (2007), 153-157.
21. Ma, D.D.D., Lee, C.S., Au, F.C.K., Tong, S.Y. and Lee, S.T., "Small-diameter silicon nanowire surfaces", ***Science,*** Vol. 299, (2003), 1874-1877.
22. Maiolo, J.R., Kayes, B.M., Filler, M.A., Putnam, M.C., Kelzenberg, M.D., Atwater, H. and Lewis, N.S., "High aspect ratio silicon wire array photoelectrochemical cells", ***Journal of the American Chemical Society***, Vol. 129, No. 41, (2007), 12346-12347.
23. Wu, Y. and Yang, P., "Direct observation of vapor-liquid-solid nanowire growth", ***Journal of the American Chemical Society,*** Vol. 123, No. 13, (2001), 3165-3166.
24. Zardo, I., Conesa-Boj, S., Estradé, S., Yu, L., Peiro, F., Roca i Cabarrocas, P., Morante, J.R., Arbiol, J. and Morral, A.F., "Growth study of indium-catalyzed silicon nanowires by plasma enhanced chemical vapor deposition", ***Applied Physics A,*** Vol. 100, No. 1, (2010), 287-296.
25. Parkhutik, V., "Porous silicon—mechanisms of growth and applications", ***Solid-State Electronics,*** Vol. 43, No. 6, (1999), 1121-1141.
26. Uhlir, A., "Electrolytic shaping of germanium and silicon", ***Bell Labs Technical Journal,*** Vol. 35, No. 2, (1956), 333-347.
27. Chartier, C., Bastide, S. and Lévy-Clément, C., "Metal-assisted chemical etching of silicon in HF–H_2O_2", ***Electrochimica Acta,*** Vol. 53, No. 17, (2008), 5509-5516.
28. Huang, Z., Buczek, N., Werner, P., Boor, J.D. and Gösele, U., "Metal-assisted chemical etching of silicon: a review", ***Advanced Materials,*** Vol. 23, No. 2, (2011), 285-308.
29. Ng, R.M., Wang , T., Liu, F., Zuo, X., He, J. and Chan, M., "Vertically stacked silicon nanowire transistors fabricated by inductive plasma etching and stress-limited oxidation", ***IEEE Electron Device Letters***, Vol. 30, No. 5, (2009), 520-522.
30. Lehmann, V., Hofmann , F., Möller, F. and Grüning, U., "Resistivity of porous silicon: a surface effect", ***Thin Solid Films,*** Vol. 255, (1995), 20-22.
31. Chang, S.w., Chuang, V.P., Boles, S.T. Thompson, C.V., "Metal-Catalyzed Etching of Vertically Aligned Polysilicon and Amorphous Silicon Nanowire Arrays by Etching Direction Confinement", ***Advanced Functional Materials,*** Vol. 20, No. 24, (2010), 4364-4370.
32. Peng, K.-Q., Yan, Y.J., Gao, S.P. Zhu, J., "Synthesis of large-area silicon nanowire arrays via self-assembling nanoelectrochemistry", ***Advanced Materials,*** Vol. 14, No. 16, (2002), 1164.
33. Li, X. and Bohn, P. "Metal-assisted chemical etching in HF/H 2 O 2 produces porous silicon", ***Applied Physics Letters,*** Vol. 77, No. 16, (2000), 2572-2574.
34. Gielis, S., Veen, M.V.D., Gendt, S.D. and Vereecken. P.M., "Silver-Assisted Etching of Silicon Nanowires", ***ECS Transactions,*** Vol. 33, No. 18, (2011), 49-58.
35. Hildreth, O.J., Lin, W. and Wong, C.P. "Effect of catalyst shape and etchant composition on etching direction in metal-assisted chemical etching of silicon to fabricate 3D nanostructures", ***ACS Nano,*** Vol. 3, No. 12, (2009), 4033-4042.
36. Abstreiter, G., Cardona, M. and Pinczuk, A., "Light scattering by free carrier excitations in semiconductors", ***in Light Scattering in Solids IV,*** Vol. 54, 1984, 5-150.
37. Sood, A., Shulin, Z., Gant, T.A., Delaney, M., Klein, M.V., Klem, J. and Morkoc, H., "Resonance Raman scattering by confined LO and TO phonons in GaAs-AlAs superlattices", ***Physical Review Letters,*** Vol. 54, No. 19, (1985), 2111.
38. Richter, H., Wang, Z. and Ley, L., "The one phonon Raman spectrum in microcrystalline silicon", ***Solid State Communications,*** "Vol. 39, No. 5, (1981), 625-629.
39. Manotas, S., Rueda, F.A., Moreno, J.D., Hander, F.B., Lemus, R.G. and Duart, J.M.M., "Determination of Stress in Porous Silicon by Micro-Raman Spectroscopy", ***Physica Status Solidi,*** Vol. 182, No. 1, (2000), 245-248.